

ENGINEERING PERSPECTIVE

CONTENTS

Research Articles

Page Number

Emmanuel KARANGWA, Pacifique TURABIMANA

Study of Subsurface damage of tungsten alloy in rotary ultrasonic grinding

99-109

Soner DURAN, Yasin COŞKUN, Derya KILIÇ, Ahmet UYUMAZ, Batuhan ZENGİN

Determination of the Load Applied to Bale Wrapping Machine Rotary Arm and Performing of Design Optimization

110-114

ENGINEERING PERSPECTIVE

An International Journal

Volume: 1

Issue: 4

31 December 2021

ENGINEERING PERSPECTIVE

Volume: 1

Issue: 4

31 December 2021



Study of Subsurface Damage of Tungsten Alloy in Rotary Ultrasonic Grinding

Emmanuel Karangwa, Pacifique Turabimana*

Mechanical Engineering Department, IPRC Gishari-Rwanda Polytechnic, Rwamagana, Rwanda

ABSTRACT

Tungsten alloy is generally used in aerospace, military defense services, the nuclear industry, and other essential fields of manufacturing due to its physical and chemical properties. As the demand for tungsten alloy increases, it demands higher requirements for the accuracy, quality, and surface integrity of tungsten alloy products. So, it is of paramount importance to study the manufacturing, processing, and testing of tungsten alloys through the power generating during ring machining, the surface, and subsurface of finished products. Grinding is an abrasive machining method that can achieve extremely fine surface finishes while retaining high dimensional and shape precision. However, the process causes subsurface damage, which affects the mechanical properties and surface quality of the machined workpiece. In this paper, the grinding simulations in Abaqus software and experiments on CNC machine on both Rotary Ultrasonic Grinding (RUG) and Conventional Grinding (CG) were carried out by Taguchi experimental design method to study the different influences of spindle speed, grinding depth, feed rate, ultrasonic frequency and amplitude on subsurface damage induced in grinding of tungsten alloy. Briefly, simulation and experiment results showed well agreement at the same time present the reduction of subsurface damage depth on ultrasonic grinding compared to conventional grinding. Also, the increase of grinding depth and feed rate and amplitude generates a high Subsurface Damage depth (SSD depth) where the increasing of spindle speed decreases the SSD depth, but ultrasonic frequency present a little effect on it.

Keywords: Tungsten alloy; Rotary ultrasonic grinding; Conventional grinding; Finite element method; Constitutive model; Subsurface damage; and Grinding force.

History

Received: 24.09.2021

Accepted: 17.11.2021

Author Contacts

*Corresponding Author

e-mail addresses: turabimanapacifique@gmail.com, pacifique.turabimana@aait.edu.et, ekarangwa25@gmail.com

Orcid numbers : 0000-0003-2422-9056 , 0000-0002-6409-235X

<http://dx.doi.org/10.29228/eng.pers.54728>

1. Introduction

Tungsten (W) is dull silver-grey metal with the highest point fusion of almost pure metal. It can be combined with other metals to form tungsten alloys to increase their strength and resistance to wear and corrosion. Because of its physical and chemical properties such as corrosion resistance, radiation safety, high hardness, and good impact efficiency, tungsten alloy is widely used in aerospace, military defense, nuclear industry, and other essential fields. In the past twenty years, due to the high strength, high density, good plasticity, and good machinability of tungsten alloy, tungsten alloy production is increasing in China. In 2003, China's density production of tungsten alloy was about 1139 tons but only six years after the product has been more than 3000 tons per year [1]. The researchers continuously review and improve the effective ways to improve tungsten alloy strength and hardness and toughness. Since conventional machining (CM) can't machine well tungsten alloy precisely due to

rapid tool wear, brittle fracture, and tool adhesion, the ultrasonic machine is applied to machine hard and brittle material [2]. Ultrasonic Machining (USM) is one of many viable machining methods that can process hard and brittle materials regardless of their electrical and mechanical properties, which are usually a constraint for other techniques. In ultrasonic machining, abrasive particles in the form of slurry strike the work surface, causing the material to be extracted. To overcome these several limitations generally, occur in static ultrasonic machining as well as conventional diamond grinding, the RUM (Rotary Ultrasonic Machining) was built. RUM is a hybrid machining process that combines USM and CM to remove material from a workpiece through microchipping and abrasive grinding [3].

As a result, it is critical to conduct a thorough study to examine SSD in grinding processes and to investigate the impact of process parameters on SSD depth. However, the subsurface damage which is introduced to substrates in manufacturing processes may seriously

deteriorate part quality. Aside from production cycle, surface accuracy, and manufacturing expense, it has an effect on operational life, secular stability, coating efficiency, and transmission performance, which has attracted a lot of attention recently [4]. Therefore, it is critical to study the factors that influence the subsurface quality of hard & brittle material in grinding. Detection, measurement, and monitoring of SSD to improve tungsten alloy machining performance and the surface is now one of the optical manufacturing industry's problems to solve [5].

The primary aim of this research is to simulate as well as perform experimental grinding processes for finding the effects of ultrasonic excitation on subsurface damage of tungsten alloy (W-Ni-Fe) to get high quality of products, improve machining efficiency, a quality life of machine parts, time-saving for machining and to minimize production costs by comparing the variations between RUG and CG at the same machining parameters.

2. Detection methods

The SSD is easily generated in the machining operation, to date, there are more researches about the techniques to evaluate and remove the SSD depth for improving the efficiency quality, a lifetime of a machined part, to reduce the cost and the time for machining based on the various methods. The destructive methods can provide measurable, accurate, and quantitative data, they cannot be used to estimate the global information of SSD in a sample. Furthermore, the sample must be destroyed, which takes time and is costly. In production methods that are rigid and production in large quantities, the detection cost is sufficient. Non-destructive methods, on other hand, are more applicable and effective. Customized parts will become more common in the future, necessitating this method for estimating the SSD initiated in a part easily. Non-destructive methods are often simpler to incorporate into a line of products and they are needed to be developed to satisfy the rising demand for high-quality manufacturing products.

2.1 Different Detection methods

The most popular method for SSD detection and observation is traditional taper polishing. A sample is cut at an angle β to the machined surface and then the cut surface of the sample is polished to minimize any damage caused by the cutting process. The polished sample is engraved to remove the polished surface's layer, exposing the SSD, which is then examined under microscopy and the SSD depth measured. The SSD depth (H) is calculated as Eq.1 [6].

$$H = L \times \sin\beta \tag{1}$$

The University of Rochester's optical manufacturing center [7] developed a dimpling method to find out SSD. This method polishes a sample part with a steel ball to create a dimple in series to reveal the SSD of the part, similar to the conventional taper polishing method. The depth of the dimple is sufficient to pass through the damage layer matrix. The SSD depth is determined by calculating the characteristic dimensions of a dimple. It is quick to operate and inexpensive. The MRF(Magnetorheological Finishing) polishing has been utilized in SSD measurement since the advent of precision ma-

chining technology [8]. Mulhern et al proposed the Bonded-Interface Technique (BIT) to look at the material deformation of metals in an indentation test [9]. Figure 1 illustrates the BIT schematics, which are subdivided into several steps. The first step was to polish the surfaces that had to be glued together; second, glue was used to bind the polished surfaces; third, the work surface was machined; finally, the bonding glue was removed, and SSD was observed using a microscope on the two polished interfaces.

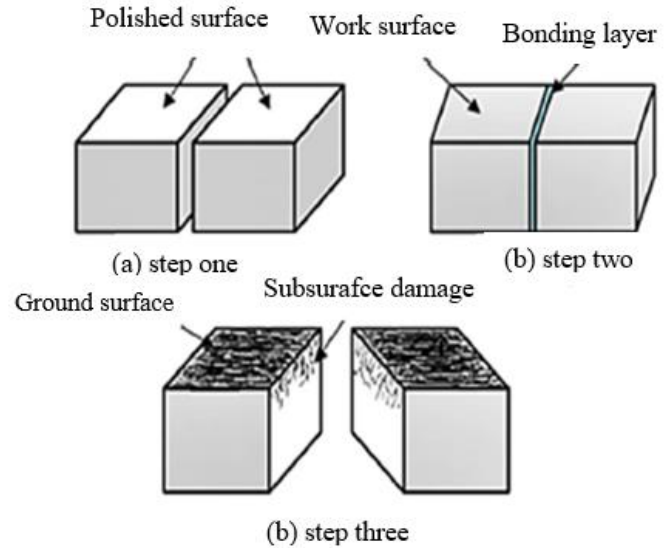


Figure 1. Schematics of bonded interface techniques

Several technologies have been proposed to detect SSD with laser scattering. Temple et al used Total Internal Reflection Microscopy (TIRM) to detect surface and subsurface damage of the transparent samples, and several other researchers applied TIRM to optical materials later [10]. Lambropoulos [11] suggested a relationship between the depth of the damage and the size of abrasive grains. Focused on indentation fracture mechanics, Wang et al [12] hypothesized that SSD formation was caused by brittle workpiece material fracture, and proposed an explicit equation to predict SSD depth as shown in equations 2.

$$\frac{\delta}{SR} = 2.326\alpha_K^{\frac{2}{3}} \left(\frac{E}{H}\right)^{\frac{2-5m}{3}} \frac{(\cot\psi)^{\frac{1}{9}}}{(\sin\psi)^{\frac{1}{2}}} \left(\frac{P}{\frac{K_c}{H^3}}\right)^{\frac{1}{6}} \tag{2}$$

where E, H, and Kc are the elastic modulus, the hardness, and the toughness of the workpiece material respectively, δ is SSD depth, SR is surface roughness, ψ is the semi-angle of the sharp cone of an abrasive grain; P is the force acting on the grain. α_K and m are numerical factors. Force P determines the ratio, yet in practical machining, it varied with process parameters, which renders the model inconvenient to use. Xiao et al [13], enhanced the model in equation 2, by stating the relation between SSD and Ra as non-linear by eliminating grain force P,

$$\delta = 3.08\alpha_K^{\frac{2}{3}} \frac{1}{(\sin\psi)^{\frac{2}{3}} E^{\frac{2m-2}{3}} K_C} SR^{\frac{4}{3}} \tag{3}$$

Feng and Zhang [14] correlated SSD depth with cutting force in the RUFM of a K9 glass. They found that SSD depth was proportional to the exponent of cutting force ($\delta = \gamma F_c^x$). Lakhdari et al [15], discovered that the SSD depth caused RUAG was 35% less than CG.

Figure 2, depicts the crack mechanism of brittle material caused by indentation with a sharp indenter, according to indentation fracture mechanics.

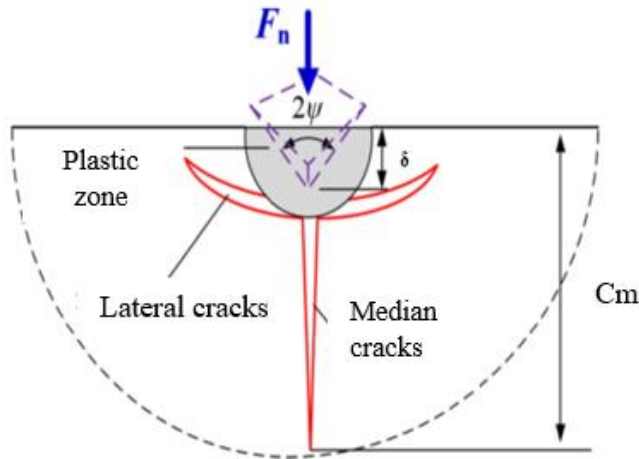


Figure 2. Diagram of crack system caused by a sharp indenter

Where F_n is maximum impact force acting on the workpiece one diamond particle, Ψ is semi angle between two opposite edges of an abrasive particle, δ is the maximum penetration depth of single abrasive particle penetration into the workpiece and C_m is a depth of median crack from the unprocessed surface. The magnitude of C_m determines the SSD characteristic in RUFM of optical glass. Based on indentation fracture mechanics, Lambropoulos et al, developed the calculation formula of C_m as flows:

$$C_m = \alpha_k \frac{2}{3} \left(\frac{E}{H_v} \right)^{\frac{2}{3}} (1-q)^{\frac{2}{3}} (\cot \Psi)^{\frac{4}{9}} \left(\frac{F_n}{K_{1c}} \right)^{\frac{2}{3}} \quad (4)$$

Where E is elastic modulus, H_v is micro-hardness, K_{1c} is fracture toughness, q is a dimensionless coefficient to correction. They found that the depth of SSD is directly proportional to the exponent of measured cutting force as seen in Equations 5.

$$d_{SSD} = \gamma F_c^x \quad (5)$$

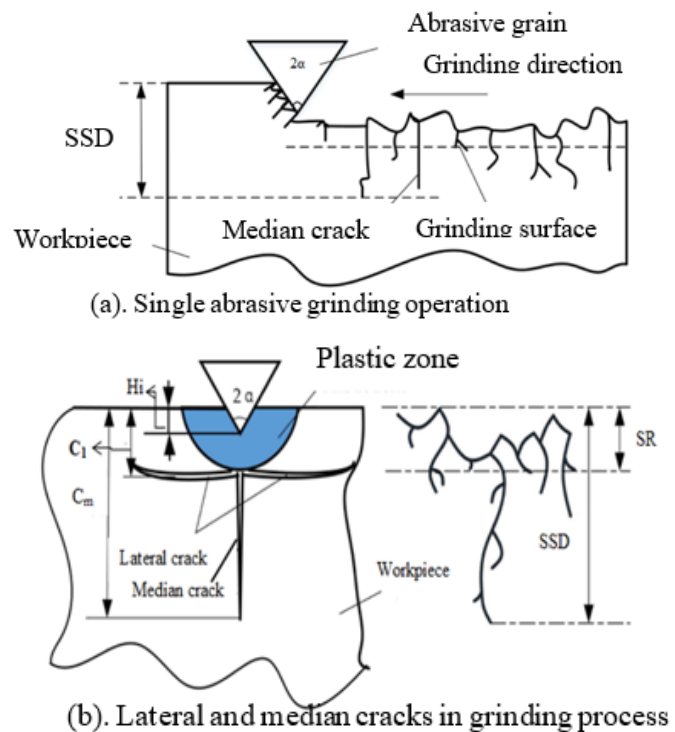
Where d_{SSD} is the predictive SSD depth, γ is the proportionality factor, and x is the index of the power function. this method has shown that under the same processing conditions, the measured cutting force in RUFM is much smaller than in CG and also the estimated cutting force follows the variance trend of SSD depth with an increase in processing parameters [16].

In the study of cracks in ceramic damage, Liu et al used utilized computational simulation to assess the degree of damage [17]. The simulation results have been shown that Ultrasonic Vibration Machining (UVM) can effectively reduce the average cutting force and reduce the cutting temperature at tooltip compared with

Con-ventional Machining (CM) and maximum misses stress show that UVM can effectively reduce the machining stress, the larger amplitude corresponds to smaller max-imum misses' stress. Moreover, the cutting effects are further improved with an increment of vibration ampli-tude under set conditions.

Linlin carried out an FEA method on silicon nitride grinding based on virtual abrasive with a truncated pol-yhedral shape to simulate the subsurface depth. The influence factors of the grinding parameters on subsur-face damage depth were analyzed. The average error between prediction and experiment results was approx-imately 9%, which validated the prediction accuracy and generalization ability of the prediction model. Also, the SSD depth increased with the increment of work-piece speed and grinding depth, while as the speed in-creased, the SSD depth decreased [18].

Yan Gu studied the theoretical analysis on the SSD model for polishing the SiC ceramic, and discovered that the contact grinding of material can be intuitively condensed into a single grit scratch processing [19], as shown in Figure 3 (a), while figure 2-3 (b), illustrates the lateral and median cracks in detail. The SSD is caused by a median crack.



The depth of median crack C_m can be calculated by property of materials, the abrasive grain geometry, and depth of penetration as:

$$C_m = 0.206 \frac{(E \times H_s)^{\frac{1}{3}}}{K_c \times \beta} (\cot \alpha)^{\frac{4}{9}} (\tan \alpha)^{\frac{4}{3}} (H_i)^{\frac{4}{3}} \quad (6)$$

Where C_m is the length of median crack from the base of the plastic region; C_l is the depth of lateral crack from the base of the plastic deformation region; H_i is the abrasive particles penetrating distance into the workpiece; α is the apex angle of abrasive grain, H_s is the scratch hardness, K_c is the fracture toughness, and β is the material factor specified by elastic recover. The SSD depth has been

calculated using mathematical relation of abrasive and workpiece as:

$$SSD = \max(C_m) \tag{7}$$

3. Methodology

The Abaqus explicitly software is used as numerical techniques on finite element analysis (FEA) method for investigating grinding simulation processes. The work-piece was modeled under a 2D model with the grinding diamond wheel. The subsurface damage depth for both grinding with and without ultrasonic was obtained from grinding simulations under the Johnson cook model. The trajectory of a single abrasive particle of the dia-mond tool is analyzed and traced using MATLAB software. For verifying the simulation results obtained from Abaqus, the experiments were conducted on a CNC machine under the same grinding parameters used in the simulation. The same diamond grinding tools were utilized in all grinding tests on both RUG and CG only the ultrasonic supply switched off for the CG pro-cess. The subsurface damage was observed by Scan-ning electron microscope-SEM and analyzed by ImageJ software after the cross-sectioning method of ground workpieces through the polishing machining. For achieving the goals of this research, the important methods and processes used are summarized in the flowing flowchart:

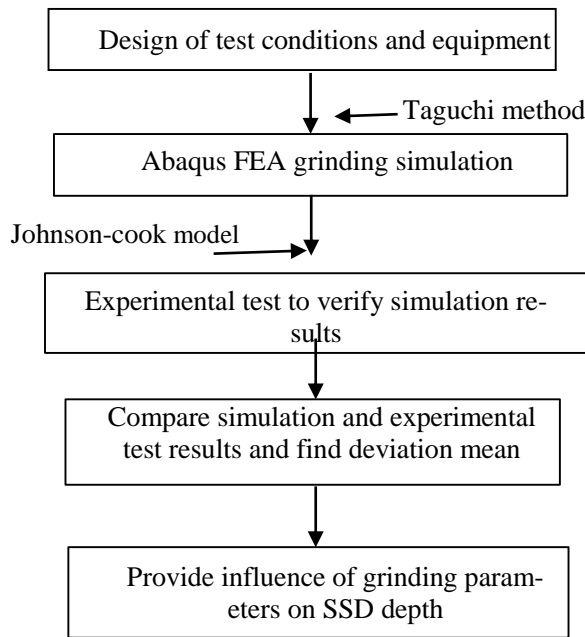


Figure 4. Proposed research methodology

Taguchi design of the experiment method is used in this study. Studying the subsurface damage of tungsten alloy on both RUG and CG, grinding depth, tool spindle speed, feed rate, ultrasonic vibration frequency, and ultrasonic vibration amplitude are selected as grinding parameters in this research. To comparing the RUG and CG results, the study must be done on similar parameters, except for RUG, ultrasonic frequency and amplitude will be applied. The detail of design plan is shown on table 1 and table 2 below:

Table 1. RUG Experiment conditions

S/N	Parameters	Value
1	Grinding depth (µm)	10, 20, 30
2	Grinding speed (rpm)	4000,5000,6000
3	Feed rate (mm/min)	20, 40, 60
4	Ultrasonic frequency (kHz)	22, 24, 26
5	Ultrasonic amplitude (µm)	1, 2, 3

Table 2. CG Experiment Conditions

S/N	Parameters	Value
1	Grinding depth (µm)	10, 20, 30
2	Grinding speed (rpm)	4000, 5000, 6000
3	Feed rate (mm/min)	20, 40, 60

3.1 FEM simulation modeling

For simulation and modeling machining processes, computational numerical models are becoming increasingly relevant [20]. Throughout the features of machining operations, the results of simulation vary significantly from experimental results, as many researchers discovered, the reason is that numerical models can only reflect physical and mechanical processes in the shear region [21]. The Johnson-Cook model for tungsten alloy is used in grinding simulation for establishing the relation involving the grinding input parameters and grinding force generated, as well as residual stress, surface morphology, and SSD. In the practical grinding process, the material removal is produced by the interaction of a large number of random particles distributed on the grinding tool head and workpiece. To make the analysis and computation process easier, a single grit approach is considered where the single grit abrasive grain simulation is used to examine the subsurface cracks during grinding tungsten alloy.

The Johnson-cook constitutive equation is the most common for modeling various machining methods, the Johnson-cook formula is as follows:

$$\sigma_s = (A + B\epsilon^n) [1 + C \ln(\frac{\dot{\epsilon}}{\dot{\epsilon}_0})] [1 - (\frac{T - T_0}{T_m - T_0})^m] \tag{8}$$

Where σ_s is the stress which causes a material to become plastic, A is the yield strength, B is the strain hardening stress constant, n is the strain hardening power constant, C denotes the strain ratio constant, m denotes the thermal softening power constant, ϵ is the strain, $\dot{\epsilon}$ is the strain rate, $\dot{\epsilon}_0$ is the value of reference rate of strain, T represents the effective temperature, T0 denotes the room temperature and Tm represents the materials' melting temperature [22].

Also, Johnson-Cook explained the model damage through erosion model by Johnson-Cook failure relying on the impact of plastic strain and presented the damage variable D shown in equation 9.

$$D = \sum \frac{\Delta\epsilon^p}{\epsilon_f^p} \tag{9}$$

Where $\Delta\epsilon^p$ represent strain's equivalent plastic in an integration phase, and ϵ_f^p represents strain's ultimate plastic, which would have the equation 10 as follow:

$$\epsilon_f^p = [D_1 + D_2 \epsilon^{D_3 \sigma^*}] [1 + D_4 \ln(\frac{\dot{\epsilon}^p}{\dot{\epsilon}_0})] [1 + D_5 T^*] \tag{10}$$

This grinding simulation 2D model is built and run by using

tungsten alloy properties and Johnson-cook pa-rameters from Bresciani on numerical modeling to re-produce fragmentation of a tungsten heavy alloy [23].

3.2 Construction FEA model

The two-dimensional (2D) model plane is used for building the workpiece and the grinding tool for envisag-ing the formation of lateral and median cracks. Alt-hough the abrasive grains on the surface of the grinding tool have a functional role in grinding. The following are assumptions of the model used:

1. During deformation, the material stayed stable and no chemical changes resulted;
2. The grinding depth was small compared to the size of grit size and the active grinding edge was greater than the depth of grinding;
3. The hardness and strength of the tool were greater compare to those of the workpiece;
4. The period of grinding simulation was severely small and the penalty approach was used in the interac-tion between abrasive and workpiece;
5. The grinding tooltip will slide on the surface of the workpiece at a constant speed and the friction fac-tor of 0.15 was used to identify the tangential and nor-mal friction.
6. For dynamic analysis, the approach of mass scaling was used for time calculation.

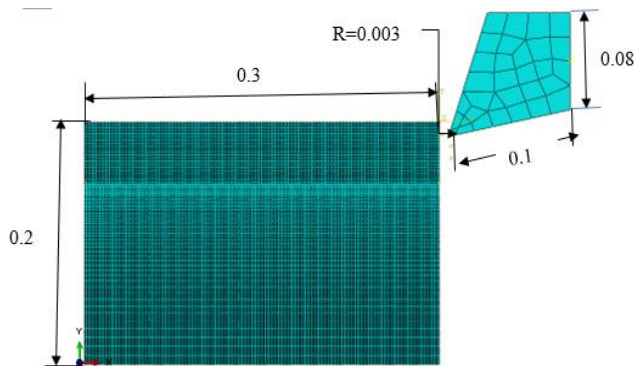


Figure 5. Abacus FEA numerical simulation model

The experimental tests were done for verifying the simulation results. To observe the SSD of tungsten alloy from experimental tests on both RUG and CG, the workpieces and grinding tools were designed and pro-duced. The specimens are made in tungsten alloy (W-Ni-Fe) while grinding tools are manufactured in dia-mond grit. The cutting wire machining was used to cut into a specimen of 12mm×10mm×3mm as the size of the experiment workpiece. The grinding tool is made in a matrix diamond wheel with 100 particle size and abrasive concentration of 200%, with 10mm× 6mm × 45 mm of the outer, inner diameter, and length of dia-mond grinding wheel respectively.

Both Rotary Ultrasonic Grinding (RUG) and Conventional Grinding (CG) tests were conducted on a Machine model called Hanchuan XK714D vertical CNC drilling and milling machine which consists primarily of an ul-trasonic spindle system, a numerical control machining, and coolant system. The ultrasonic spindle system comprises a control panel, power supply, electrical mo-tor, and machining tool in a tool holder. The data ac-quisition system or numerical control machining system comprises a

specimen, machine table, fixture, dyna-mometer, A/D converter, amplifier, and computer while the coolant system comprises with coolant tank, pump, valve, flowrate gauge, pressure regulator, and pressure gauge.



Figure 6.a. Hanchuan XK714D CNC drilling and Mill-ing with all accessories

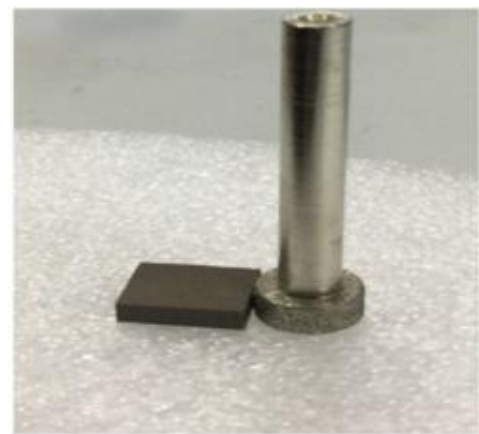


Figure 6.b. Grinding tool and workpiece used in the study

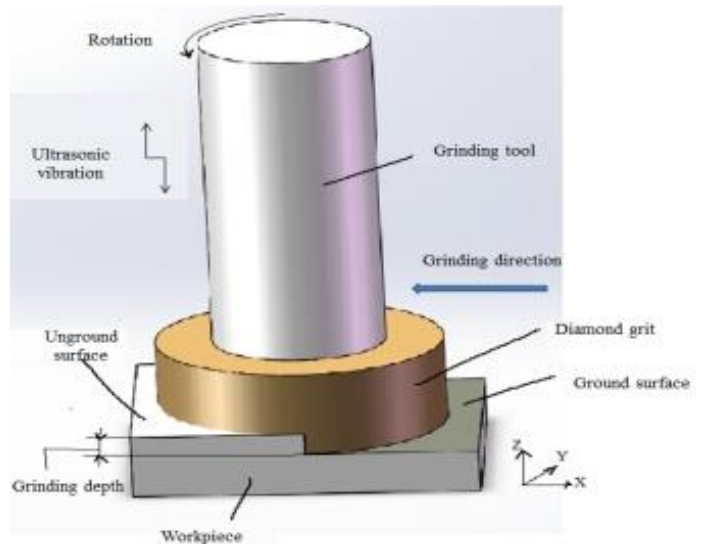


Figure 6.c. Designed grinding direction & position



Figure 6.d. Experimental grinding process

3.3 Polishing process and observation of subsurface damage by using SEM

The ground workpieces of $12\text{mm} \times 10\text{mm} \times 3\text{mm}$ are cut into two equal parts by cutting wire at the surface of $12\text{mm} \times 10\text{mm}$, and at that time the two-cut polishing backing sheets have the size of $12\text{mm} \times 5\text{mm} \times 3\text{mm}$ of length, width, and thickness respectively. The processed sample surface and the same size surface of the backing sheet are bonded together with the glue layer. During bonding, the two samples, the pressure is required to make good bonding joint and tight. The bonding in the pair is shown in Figure 7.

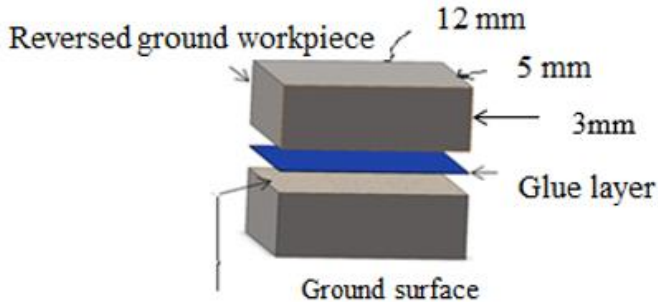


Figure 7. Bonding process and polishing machining

To detect the subsurface damage generated during the grinding process, each ground workpiece was polished on a polishing machine by using 320Cw, 800Cw, 1500Cw, and 2000Cw abrasive polishing paper by using the cross-section polishing method. The grinding time is long enough to ensure the removal of the damage caused by the wire cutting process. After polishing the glue layer is

dissolved and the sample is cleaned. The samples were preserved and then observed by SEM and the ImageJ software is used to measure the depth of crack recorded. The Subsurface damage evaluation index was based on maximum damage layer depth which was taken as SSD depth, these damage evaluation indexes were recorded during SEM. Then the sub-surface damage obtained on grinding with ultrasonic and conventional grinding were compared.

4. Results and discussion

The existence of subsurface damage seriously affects the performance and life of the workpiece products. In this section, through the orthogonal array tests, the influence of grinding parameters on the depth of subsurface damage is systematically studied. Based on the subsurface damage results obtained, the subsurface damage characteristics are summarized and analyzed, which can provide a basis for effectively reducing the subsurface damage. Both simulation and experimental SSD depth results are obtained by taking the maximum depth of subsurface damage which are summarized in table 3. The analysis was done based on Orthogonal Experiment Assistant (OEA) software for the Taguchi experiment method on designed simulation grinding parameters.

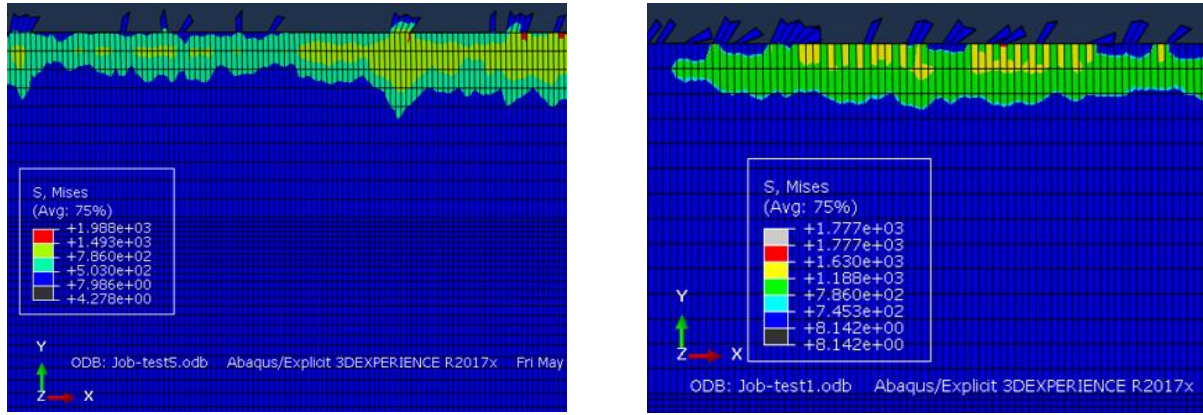
4.1 Simulation SSD depth results

The overall tensile stress is the most key factor monitoring the materials' brittle failure as per fracture mechanics theory [24]. A brittle fracture happens when a point's maximum tensile stress exceeds the limit stress of a single stress state. Its key aim is to extract material by fracturing and friction, then here in the case of tungsten alloy, the damage appears on the workpiece where if the tensile strength exceeds 786 MPa as bending strength material [18]. As a result, the stress on the grinding surface of the workpiece needs to be assessed. To identify various areas of stress, the counter colors & lines are processed. Once the von mises stress of the built model is over 786 MPa. The magnitude of SSD depth is the maximum SSD depth measured on the ground workpiece by locating the corresponding region in the contour color using the node distance method [25].

The SSD depth simulation results obtained on both RUG and CG are presented in Figure 8. Figure 8 shows some screenshot photos taken to indicate the surface and SSD depth in simulation at different parameters

4.2 Experimental SSD depth results

To verify FEA simulation results, the grinding experiments on both RUG and CG have been conducted three times to confirm the simulation results. The experimental SSD depth results obtained by taking the maximum depth of subsurface damage among of five points measured for each ground and polished work-piece on a scanning electron microscopy for three repeated tests are summarized in table 3.



a. RUG at Gd=10μm, Vs=4000rpm, Vw=20mm/min, f=22 kHz, a= 1μm, SSD depth=17.65μm b. CG at Gd=10μm, Vs=4000rpm, Vw=20mm/min, SSD depth=21.50μm

Figure 8. Surface morphology of SSD depth on both RUG and CG

Table3 (a): RUG Orthogonal test simulation and SSD experimental depth results

Test	Gd (μm)	Vs (rpm)	Vw (rpm)	f (rpm)	a (μm)	SIM.SSD depth (μm)	EXP. SSD depth (μm)				Deviation (%)
							T1	T2	T3	Average	
1	10	4000	20	22	1	17.65	17.20	18.80	13.5	16.50	6.52
2	10	5000	40	24	2	16.45	16.80	20.10	16.2	17.70	-7.60
3	10	6000	60	26	3	19.40	20.50	16.35	18.95	18.60	4.12
4	20	4000	20	24	2	20.12	19.20	17.45	17.95	18.20	9.54
5	20	5000	40	26	3	18.87	24.10	25.70	21.30	23.70	-25.60
6	20	6000	60	22	1	19.65	16.40	20.18	18.93	18.50	5.85
7	30	4000	40	22	3	23.37	30.18	29.50	27.32	29.00	-24.09
8	30	5000	60	24	1	26.26	23.43	26.40	22.77	24.20	7.84
9	30	6000	20	26	2	16.85	15.78	18.26	16.06	16.70	0.89
10	10	4000	60	26	2	23.75	23.90	24.48	21.52	23.20	2.32
11	10	5000	20	22	3	14.05	15.45	13.65	12.90	14.00	0.36
12	10	6000	40	24	1	14.49	14.00	15.85	14.25	14.70	-1.45
13	20	4000	40	26	1	23.36	22.15	20.40	17.45	20.00	14.38
14	20	5000	60	22	2	22.65	24.70	22.50	20.30	22.50	0.66
15	20	6000	20	24	3	16.05	15.60	13.80	15.18	14.86	7.41
16	30	4000	60	24	3	30.73	30.68	30.50	27.92	29.70	3.35
17	30	5000	20	26	1	20.80	17.50	19.40	19.20	18.70	10.10
18	30	6000	40	22	2	21.76	23.00	20.79	20.71	21.50	1.19
Average deviation											0.88

Table3 (b). CG orthogonal experiment SSD depth results

Test	Gd (μm)	Vs (rpm)	Vw (rpm)	SIM.SSD depth (μm)	EXP. SSD depth (μm)				Deviation (%)
					T1	T2	T3	Average	
1	10	4000	20	21.45	25.70	26.15	22.40	24.75	13.33
2	10	5000	40	22.40	26.20	24.50	24.60	25.10	10.76
3	10	6000	60	26.65	27.30	28.45	23.60	26.45	-0.76
4	20	4000	40	31.00	40.15	35.46	39.29	38.30	19.06
5	20	5000	60	34.35	39.28	36.78	35.09	37.05	7.29
6	20	6000	20	21.35	20.19	23.45	22.81	22.15	3.61
7	30	4000	60	40.15	45.69	46.38	41.28	44.45	9.67
8	30	5000	20	26.25	30.90	28.10	29.85	29.95	12.35
9	30	6000	40	28.10	34.15	27.45	31.10	30.90	9.06
Average deviation									9.38

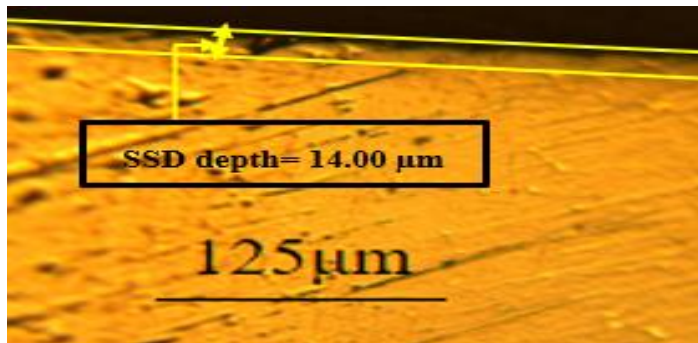
4.3 Trend analysis and influence effects of grinding parameters on SSD depth

a. Graphical trend on each parameter

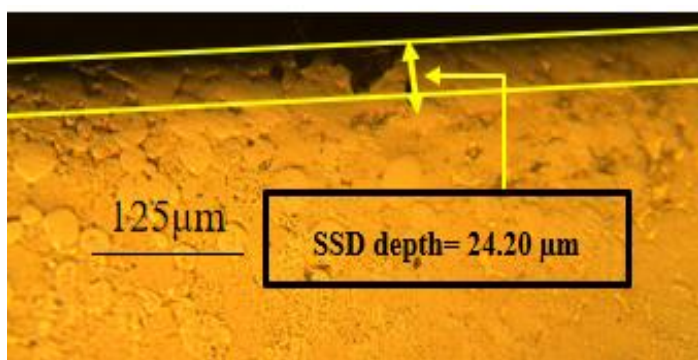
The order of influencing of every parameter on RUG SSD depth is feed rate, grinding depth, spindle speed, amplitude, frequency, while for CG SSD depth, it is feed rate, grinding depth, spindle speed respectively for both simulation and experiment as shown on the figure 9. The analysis of the influence of different parameters for each level on SSD depth brings the optimized combination of processing parameters.

It can be observed that the SSD depth increases with increasing grinding depth, feed rate, and ultrasonic amplitude while the SSD decreases with increasing grinding spindle speed; the ultrasonic vibration frequency has a little effect on SSD depth which is similar to the numerical simulation result obtained.

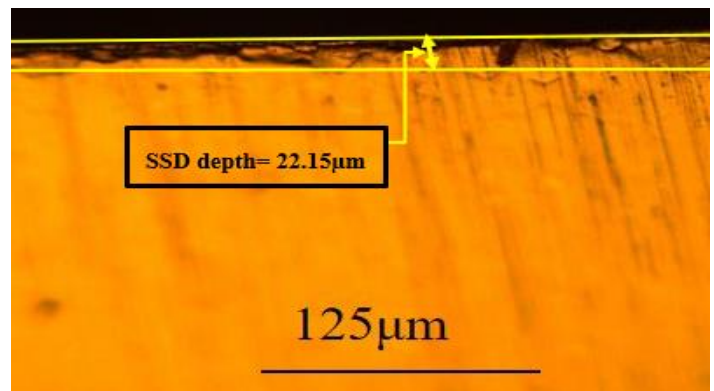
According to the range of each parameter and the trend graph, the optimal combination of the SSD depth on RUG is Vw1Gd1Vs3a1f2 and Vw1Gd1Vs3 on RUG and CG respectively. According to both numerical simulation and experimental orthogonal test method results, to reduce the subsurface damage depth during selecting machining grinding parameters, the Vw1Gd1Vs3a1f2 optimized combination is suggested, where the grinding depth is 10 μm, spindle speed is 6000 rpm, feed rate 20mm/min, the ultrasonic frequency of 24 kHz, and ultrasonic amplitude of 1μm.



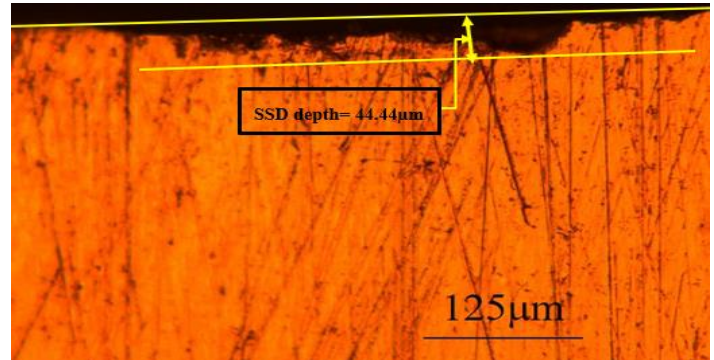
a. RUG at Gd=10μm, Vs=5000rpm, Vw=20mm/min, f=22 kHz, a=1μm



b. RUG at Gd=30μm, Vs=5000rpm, Vw=60mm/min, f=24 kHz, a=1μm



c. CG at Gd=20μm, Vs=6000rpm, Vw=20mm/min



d. CG at Gd=20μm, Vs=4000rpm, Vw=40mm/min

Figure 9. Present SEM-SSD depth taken on different parameters

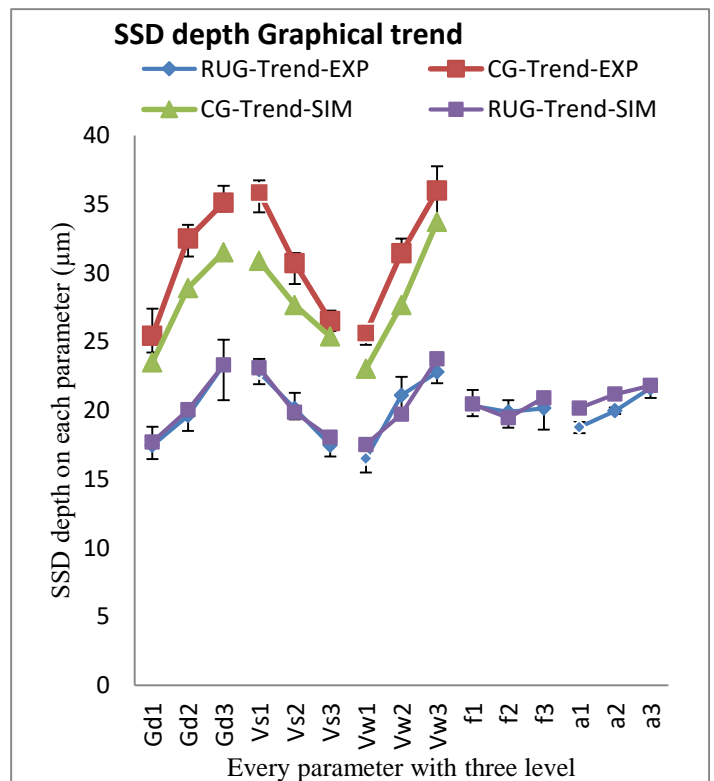


Figure 10. Graphical trend on each parameter on SSD depth both simulation and experiment

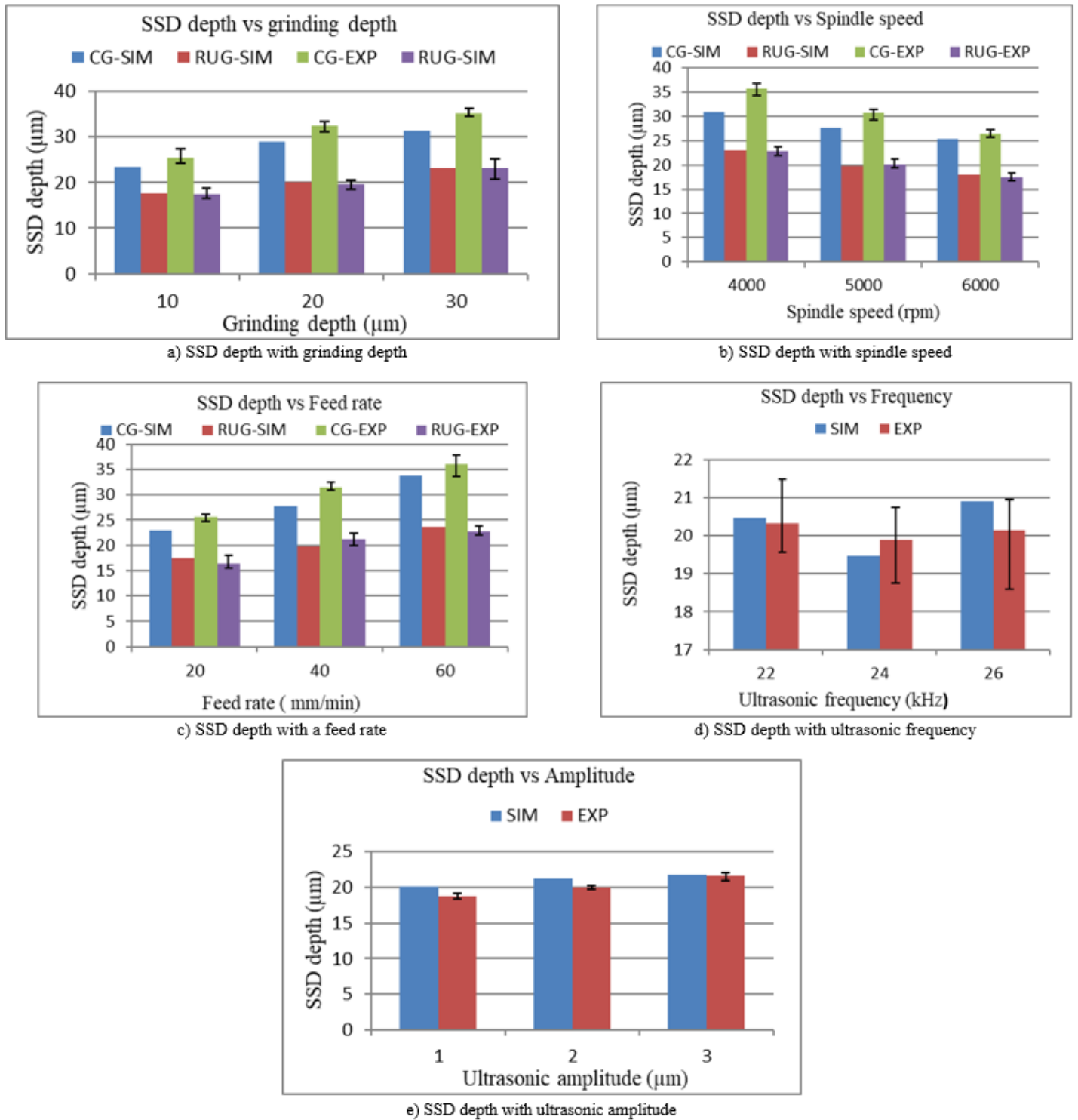


Figure 11. SSD Depth on both simulation and experiment grinding parameters

Hence, as mentioned above, the experiment results of grinding depth, feed rate, and spindle speed on subsurface damage depth are well consistent with those existing experimental works to Yao et al [26] and [27]. The results show that the subsurface damage depth values obtained under the rotary ultrasonic grinding methods are significantly smaller than those of ordinary grinding methods. Therefore, it can be inferred that under certain processing conditions,

the introduction of ultrasonic vibration effectively reduces the generation of sub-surface damage during the grinding process and obtains a better grinding surface. Therefore, this report believes that at the smaller grinding depth, feed rate, and higher spindle speed, the subsurface damage in grinding of tungsten alloy should be small, and the grinding surface integrity is better. It can be assumed that under certain processing conditions, the strength of ultrasonic vibration

has an important impact on the subsurface damage, and the appropriate vibration intensity can more effectively reduce the generation of subsurface damage in W-Ni-Fe rotary ultrasonic grinding.

b. Effect of grinding parameters on subsurface damage

Refer to the statistical analysis done on each parameter with each level on the influence effect of grinding depth, spindle speed, feed rate, ultrasonic frequency, and amplitude on subsurface damage through measuring SSD depth on both FEA simulations and experimental tests for both RUG and CG SSD depth is presented in figure 11.

The grinding depth plays an important role in SSD depth in brittle and ductile material grinding. The SSD depth grows in proportion to the grinding depth. When the grinding depth increases, the thickness of the material contacted by the abrasive particles on the outer side of the grinding wheel becomes larger, and the number of abrasive particles involved in the grinding increases, leading to an increase in the median crack damage as shown in figure 11(a). When the feed speed increases, the median crack depth becomes larger. With the increase of the feed speed, the actual grinding thickness of a single abrasive grain in the feed direction increases and leads to an increase in the SSD depth as shown in figure 11(c). Also, with the increase of the tool feed speed, the abrasive-material contact force would generally increase, thus deteriorating the stress state in the interior material. The lateral cracks produced by the previous abrasives would provide the effects for the increased force imposed on the subsequent abrasives. On the other hand, the lateral grinding depth of each abrasive would decrease with the increased grinding spindle speed, reducing the mechanical loads exerted on the material which generates the reduction of SSD depth as illustrated in figure 11(b).

The superposing of an ultrasonic vibration would lead to the maximum grinding depth of each abrasive increased by the value of amplitude, this increasing of depth would expose both abrasive and workpiece to a high mechanical load which increases the depth of median crack [28]. This is a clear reason for the increment of SSD depth for increasing the ultrasonic amplitude as shown in figure 11 (e).

Refer to the simulation and experimental tests results, the effects of grinding tool speed through spindle speed, grinding depth, feed rate, ultrasonic frequency, and ultrasonic amplitude on subsurface damage are consistent on both simulation and experiment processes. Also, the introduction of ultrasonic grinding shows that the values of subsurface damage reduced compared to those conventional grinding. Therefore, the feed rate had the largest impact, followed by grinding depth, spindle speed, amplitude, and final ultrasonic frequency had little effect on SSD depth. Through subsurface damage orthogonal array simulation and experiment results, the comparison between RUG and CG is easily by correlating the test results obtained on analogous grinding conditions means the same parameter and level on grinding depth, spindle speed, and feed rate. This comparison showed that the RUG SSD depth reduced about 27.79 % and 34.85 % of simulation and experimental tests respectively compared to CG SSD. And also presented a good agreement as to the average deviation on the SSD depth, which is 0.88% and 9.39% on RUG and CG respectively.

5. Conclusions

Based on the study of subsurface damage of tungsten alloy (W-Ni-Fe) done, shows a good agreement with FEA simulation and experiment tests conducted on both rotary ultrasonic grinding and conventional grinding machining processes. The complete work and related conclusions on simulation processes, experimental grinding tests, subsurface damage detection, and influence effects of grinding parameters are summarized as follows:

a. On both FEA numerical simulations and experiment tests, the introduction of rotary ultrasonic vibration (RUG) can effectively save the labor energy required through the grinding force in the grinding process and also under the same grinding parameters on both simulation and experiment processes, results show that the introduction of rotary ultrasonic vibration can effectively reduce the subsurface damage.

b. Through different grinding parameters tests of W-Ni-Fe on both RUG and CG, show that the grinding depth, feed rate, spindle speed, and ultrasonic amplitude have more effect on subsurface damage but ultrasonic frequency presents a little effect. Also, the feed rate is the most factor affecting the subsurface damage.

c. In this study, the W-Ni-Fe material is removed by brittle fracture.

In general, to reduce the grinding force and subsurface damage generated during the grinding process, not only reasonable process methods and processing parameters must be selected, but also tungsten alloy should be clarified as much as possible during the preparation of material. For the industry, this research has an immediate impact if the subsurface damage model is applied. By controlling the machining parameters, accepting the level of subsurface damage which can obtain according to the requirement of customers, and the number of defective parts should be reduced and increasing the productivity. The lower the grinding depth and feed rate, the higher the grinding spindle speed, and neither too small nor too big ultrasonic frequency and amplitude should reduce the subsurface damage depth.

Conflict of Interest Statement

The authors must declare that there is no conflict of interest in the study.

CRediT Author Statement

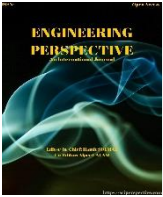
Emmanuel Karangwa: Conceptualization, Supervision, Writing-original draft, Writing-revised-paper

Pacifique Turabimana: Conceptualization, Writing-original draft, Validation, Writing-original draft, Writing-revised-paper

References

1. Y. Şahin, "Recent Progress in Processing of Tungsten Heavy Alloys," *J. Powder Technol.*, vol. 2014, pp. 1–22, 2014.
2. L. Jieqiong, H. Jinguo, L. Mingming, G. Yan, and Z. Wenhui, "Development of nonresonant elliptical vibration cutting device based on a parallel piezoelectric actuator," *AIP Adv.*, vol. 7, no. 3, 2017.
3. Z. J. Pei and P. M. Ferreira, "Experimental investigation of rotary ultrasonic face milling," *Int. J. Mach. Tools Manuf.*, vol. 39, no. 8, pp. 1327–1344, 1999.
4. Z. J. Pei, P. M. Ferreira, S. G. Kapoor, and M. Haselkorn, "Rotary ultrasonic machining for face milling of ceramics," *Int. J. Mach. Tools*

- Manuf., vol. 35, no. 7, pp. 1033–1046, 1995.
5. W. Cong, Z. Pei, and M. S. Engineering, “Handbook of Manufacturing Engineering and Technology,” *Handb. Manuf. Eng. Technol.*, no. Legge 1966, pp. 1–19, 2013.
 6. J. F. Yin, Q. Bai, and B. Zhang, “Methods for detection of subsurface damage: A review,” *Chinese J. Mech. Eng. (English Ed.)*, vol. 31, no. 3, 2018.
 7. Y. Zhou, P. D. Funkenbusch, D. J. Quesnel, D. Golini, and A. Lindquist, “Effect of Etching and Imaging Mode on the Measurement of Subsurface Damage in Micro ground Optical Glasses,” *J. Am. Ceram. Soc.*, vol. 77, no. 12, pp. 3277–3280, 1994.
 8. O. Al, H. Jeong, B. H. Koo, and C. G. Lee, “Mössbauer spectra of MnFe,” vol. 4, pp. 1129–1132, 2010.
 9. T. O. Mulhearn, “The deformation of metals by Vickers-type pyramidal indenters,” *J. Mech. Phys. Solids*, vol. 7, no. 2, pp. 85–88, 1959.
 10. C. F. Kronenberg and K. C. Jungling, “Subsurface damage identification in optically transparent materials using a non-destructive method,” *Appl. Opt.*, vol. 33, no. 19, p. 4248, 1994.
 11. J. C. Lambropoulos, “w, 1.4,” vol. 4680, no. 1987, 2000.
 12. J. Wang, Y. Li, J. Han, Q. Xu, and Y. Guo, “Evaluating subsurface damage in optical glasses,” *Journal of the European Optical Society*, vol. 6, 2011.
 13. H. Xiao, Z. Chen, H. Wang, J. Wang, and N. Zhu, “Effect of grinding parameters on surface roughness and subsurface damage and their evaluation in fused silica,” *Opt. Express*, vol. 26, no. 4, p. 4638, 2018.
 14. C. Zhang, J. Zhang, and P. Feng, “Mathematical model for cutting force in rotary ultrasonic face milling of brittle materials,” *Int. J. Adv. Manuf. Technol.*, vol. 69, no. 1–4, pp. 161–170, 2013.
 15. F. Lakhdari, D. Bouzid, N. Belkhir, and V. Herold, “Surface and subsurface damage in Zerodur® glass-ceramic during ultrasonic-assisted grinding,” *Int. J. Adv. Manuf. Technol.*, vol. 90, no. 5–8, pp. 1993–2000.
 16. J. Wang, C. Zhang, P. Feng, and J. Zhang, “A model for prediction of subsurface damage in rotary ultrasonic face milling of optical K9 glass,” *Int. J. Adv. Manuf. Technol.*, vol. 83, no. 1–4, pp. 347–355, 2016.
 17. Y. Liu, X. Wu, Q. Guo, C. Jiang, F. Song, and J. Li, “Experiments and numerical simulations of thermal shock crack patterns in thin circular ceramic specimens,” *Ceram. Int.*, vol. 41, no. 1, pp. 1107–1114, 2015.
 18. L. Wan, Z. Liu, Z. Deng, L. Li, and W. Liu, “Simulation and experimental research on subsurface damage of silicon nitride grinding,” *Ceram. Int.*, vol. 44, no. 7, pp. 8290–8296, 2018.
 19. X. Jing, S. Maiti, and G. Subhash, “A new analytical model for estimation of scratch-induced damage in brittle solids,” *J. Am. Ceram. Soc.*, vol. 90, no. 3, pp. 885–892, 2007.
 20. D. Mourtzis, M. Doukas, and D. Bernidaki, “Simulation in manufacturing: Review and challenges,” *Procedia CIRP*, vol. 25, no. C, pp. 213–229, 2014.
 21. V. Kushner and M. Storchak, “Modelling the material resistance to cutting,” *Int. J. Mech. Sci.*, vol. 126, no. March, pp. 44–54, 2017.
 22. W. Grzesik, P. Niesłony, and P. Laskowski, “Determination of Material Constitutive Laws for Inconel 718 Superalloy Under Different Strain Rates and Working Temperatures,” *J. Mater. Eng. Perform.*, vol. 26, no. 12, pp. 5705–5714, 2017.
 23. L. M. Bresciani, A. Manes, T. A. Romano, P. Iavarone, and M. Giglio, “Numerical modeling to reproduce fragmentation of a tungsten heavy alloy projectile impacting a ceramic tile: Adaptive solid mesh to the SPH technique and the cohesive law,” *Int. J. Impact Eng.*, vol. 87, pp. 3–13, 2016.
 24. J. Li, F. Song, and C. Jiang, “Direct numerical simulations on crack formation in ceramic materials under thermal shock by using a non-local fracture model,” *J. Eur. Ceram. Soc.*, vol. 33, no. 13–14, pp. 2677–2687, 2013.
 25. Y. Chen, “Prediction of Subsurface Damage During Machining Nickel-Based Superalloys,” 2013.
 26. D. Lv, Y. Huang, Y. Tang, and H. Wang, “Relationship between subsurface damage and surface roughness of glass BK7 in rotary ultrasonic machining and conventional grinding processes,” *Int. J. Adv. Manuf. Technol.*, vol. 67, no. 1–4, pp. 613–622, 2013.
 27. W. Gu, Z. Yao, and H. Li, “Investigation of grinding modes in horizontal surface grinding of optical glass BK7,” *J. Mater. Process. Technol.*, vol. 211, no. 10, pp. 1629–1636, 2011.
 28. D. Lv, H. Wang, W. Zhang, and Z. Yin, “Subsurface damage depth and distribution in rotary ultrasonic machining and conventional grinding of glass BK7,” *Int. J. Adv. Manuf. Technol.*, vol. 86, no. 9–12, pp. 2361–2371, 2016.



Determination of the Load Applied to Bale Wrapping Machine Rotary Arm and Performing of Design Optimization

Soner Duran¹, Yasin Coşkun¹, Derya Kılıç¹, Ahmet Uyumaz^{2*}, Batuhan Zengin²

¹ Kayhan Ertuğrul Machinery R & D Department, Burdur, 15040, Turkey

² Mechanical Engineering Department, Faculty of Engineering and Architecture, Burdur Mehmet Akif Ersoy University, Burdur, 15030, Turkey

ABSTRACT

In this study, it was aimed to determine the optimum design for bale wrapping machine rotary arm. Determination of the force has been ensured by determining of the hydraulic motor outlet pressure acting the bale wrapping arm and verifying these values with the help of mathematical equations. It was targeted to decrease the displacement and stress values via the changing of bale wrapping arm pipe thickness (6,5,4,3 and 2 mm) that does not restrict the machine's mobility. Static constructional analyses of different arm designs have been conducted with Ansys Workbench simulation program. Maximum displacement values were determined as 2.2677, 2.9035, 3.9552, 6.0299 and 11.636 mm with 6,5,4,3 and 2 mm pipe thickness respectively. Maximum stress values were obtained as 20.196, 26.651, 36.453, 55.491 and 98.806 MPa with 6,5,4,3 and 2 mm pipe thickness respectively. It can be suggested that 3mm pipe thickness could be safely used for rotating arms. It was seen that maximum stress and displacement values decreased with the increase of pipe thickness.

Keywords: Bale Machine Wrapping Arm, Design, Optimization, Stress

History

Received: 05.10.2021
Accepted: 14.12.2021

Author Contacts

*Corresponding Author

e-mail addresses : sonerduran@kayhanertugrul.com.tr , yasincoskun@kayhanertugrul.com.tr , deryakilic@kayhanertugrul.com.tr , ayumaz@mehmetakif.edu.tr* , bthnzngn197@gmail.com

Orcid numbers : 0000-0001-7531-909X¹, 0000-0002-3820-7934¹, 0000-0002-2018-0657¹, 0000-0003-3519-0935^{2*}, 0000-0001-9217-7839²

<http://dx.doi.org/10.29228/eng.pers.55670>

1. Introduction

Livestock has a significant importance over the development of agriculture sector and it changes according to the increment on usage ability of the technology of the small business in parallel. Furthermore, small business channel into silo feeds, which are cheap and qualified, provides more economical production opportunities [1].

The water and nutrition content on qualified food is important. For that reason, the silage is the leading of coarse fodder. Silage meets the feed needs of ruminants such as cattle, sheep and goats. It is obtained as a result of fermentation with the effect of lactic acid bacteria by leaving the high moisture feeds stored in the silos in the oxygen-free environment [2]. It is the only succulent and economical coarse fodder which can be provided while in winter time [3]. One of the main factors of production of qualified feed is the usage of technology. Harvest is the leading of the stages that is used technology on the production of coarse fodder. Baling which is used while harvesting is a process providing storage of the stalks and forage crops in lowest stage and shortest time without any defect [4].

Silage production is important in our country because the meadow fields are limited, the grazing season is limited and the need for roughage in the winter months is an important problem. If the coarse fodder is succulent in winter time, the productivity of the animals is kept along whole year. In the seasons which have abundant of succulent feeds, silage is obtained by ensiling the surplus of grass along with the pulse, gramine, forage crops and leftovers of industrial crops.

Silage provides the animals to be feed in well and economical when no succulent feeds are not in winter seasons. It reduces the cost of storage and storing problems. 15 tons of green crops can be stored in place of 2 tons of dry crops. The crops for silage can be harvested in short time and provides suitable time for the next cultivation.

With the drying of the green crops, leafery and stalks go down. Since the stalks have been dried, they are not eaten by the animals willingly. But in ensiling, no lose on the food value of the feeds and they are eaten eagerly. The crop which will be converted to silage need to be harvested in the time when the quality of the crop and its ensiling ability is maximum. During harvesting, need to be cared that stone, soil, wire etc. will not mix in the crop. The humidity of

the plant is very important. The lower or higher humidity in the plant may reduce the quality of the silage and cause decomposition. If no water comes out when the crop is crushed but humidity is felt in the hand, it means that humidity rate is among 60-67%, so the fodder can safely be ensiled [5-6].

Although the performance of silage wrapping has been comprehensively studied by some scientists [7-9], studies on parameter optimization for a cylindrical bale wrapping machine are so rare. In order to support the development on silage technology of the bales made by grass, clover, corn etc., a drum type cylindrical bale wrapping machine based on wrapping silage with stretch film (the drum drives the stretch film to rotate around the round bale, while the carrier rollers move the round bale to rotate) can be designed and arranged according to round bales of different characteristics.

In this study, with the theoretical analysis and experimental study on the wrapping arm of the bale wrapping machine, the round bale wrapper of grass, clover, corn etc., static structural analysis has been carried out on the arm by considering the maximum torque and pressure values which will be applied by the hydromotor. The arm of the bale wrapper is mounted with a flanged and bolted connection to the part where the hydromotor moves, Optimum arm design is aimed by examining the tensile and displacement of the pipe.

2. Material and Method

The rotational movement required for the arms of the bale wrapping machine is provided with the help of a fixed displacement hydromotor. The technical specifications of the hydromotor are given in Table 1.

Table 1. The technical specifications of the hydromotor

Displacement (cm ³)	158.7
Nominal pressure (bar)	140
Maximum pressure (bar)	210
Maximum torque (Nm)	307
Maximum speed (rpm)	380

The schematic representation of the arm system of the bale wrapping machine is shown in Figure 1.

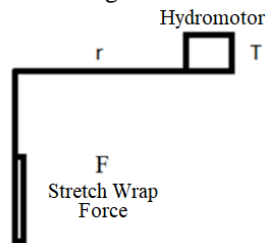


Figure 1. The schematic representation of the arm system of the bale wrapping machine

In the study, static structural analysis was carried out on the arm, taking into account the maximum torque and pressure values to be applied by the hydromotor. The arm of the bale wrapping machine is mounted to the part where the hydromotor moves, with flange and bolted connection. In this study, it is aimed to design the optimum arm by examining the tension and displacement of the pipe.

Figure 2 shows the rotating arm of the bale wrapping machine. Figure 3 shows the position of the hydromotor and the rotating wrapping arms.

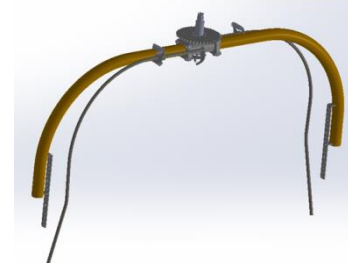


Figure 2. Rotating arm of the bale wrapping machine

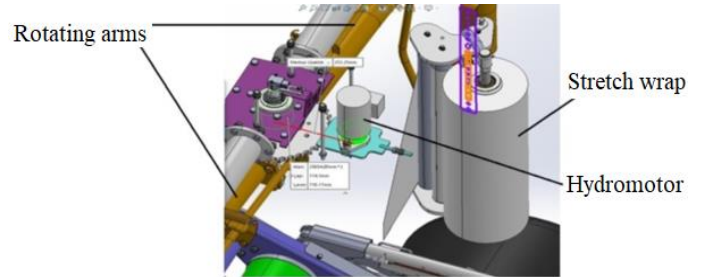


Figure 3. Position of the hydromotor and the rotating wrapping arms

The Eq.(1) is used to calculate the torque value produced by the hydromotor. In Eq.(1), V denotes engine displacement (cm³), η_{mh} denotes hydromechanical efficiency, and ΔP (bar) denotes pressure difference.

$$M_{ab} = \frac{\Delta P \cdot V \cdot \eta_{mh}}{20 \cdot \pi} \quad (1)$$

Calculation of power (kW) is performed by Eq.(2). Q in the equation gives the flow rate (l/min), η_{ges} gives the total efficiency.

$$P_{ab} = \frac{\Delta P \cdot Q}{600 \cdot \eta_{ges}} \quad (2)$$

The determination of the system flow rate is done with the help of Eq.(3). Here η_v represents the volumetric efficiency and n represents the hydromotor speed.

$$Q = \frac{n \cdot V \cdot \eta_v}{1000} \quad (3)$$

The force acting on the vertical of the bale wrapping arm is determined by dividing the maximum torque the hydromotor is exposed to by the arm length. The calculation of this force value is provided by Eq.(4). Centrifugal force of the rotating arms was also computed.

$$F = \frac{T}{r} \quad (4)$$

2.1 Designing of the different rotating arms

One of the most important design parameters for rotating arm in the bale wrapping machine is the pipe thickness. The outer diameter of the original produced pipe used is 90 mm and the thickness is

5 mm. Static structural analysis was carried out in 5 different pipe thicknesses (2, 3, 4, 5 and 6 mm) in order to determine the maximum stress and displacement amounts that may occur in the arm depending on the force applied to the arm during the wrapping of the bale and to improve the design. While the rotating arms are being designed, the 32 kg stretch required for wrapping the bale is included in the design. Weight of the stretch was considered in the analysis. St 37 steel was used as the pipe material. Mechanical and physical properties of St 37 steel are given in Table 2. The technical drawing dimensions of the rotating arm of the bale wrapping machine are given in Figure 4.

2.2 Analysis

Rotating arms with different pipe thicknesses are modeled in Solidworks program. Then, the rotating arms in the Ansys Workbench program were subjected to static analysis. In the analysis, first of all, St 37 steel material assignment was performed on the program. The mesh layer was created in the Ansys program of the rotating arm, which was previously designed in five dimensions.

Table 2. Some mechanical and physical properties of St 37 steel (S235JR) [10-13]

Density (kg/m ³)	7800
Modulus of elasticity (MPa)	210000
Elongation (%)	22
Tensile strength (MPa)	360
Yield strength (MPa)	235
Poisson ratio	0.28

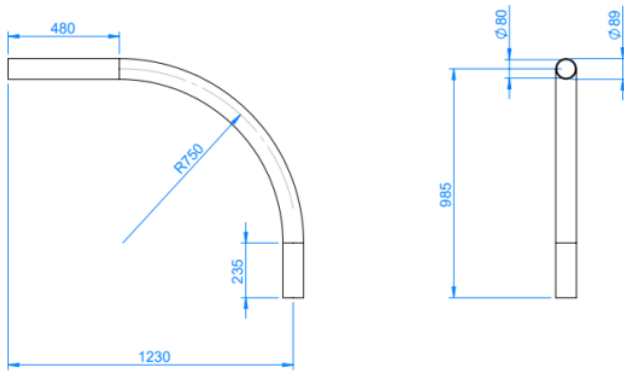


Figure 4. Technical drawing dimensions of the rotating arm of the bale wrapping machine

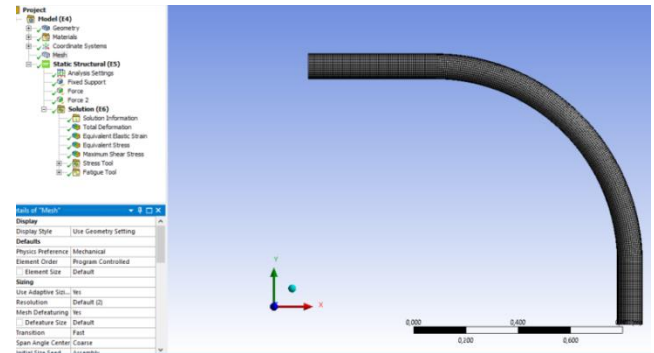


Figure 5. Mesh structure

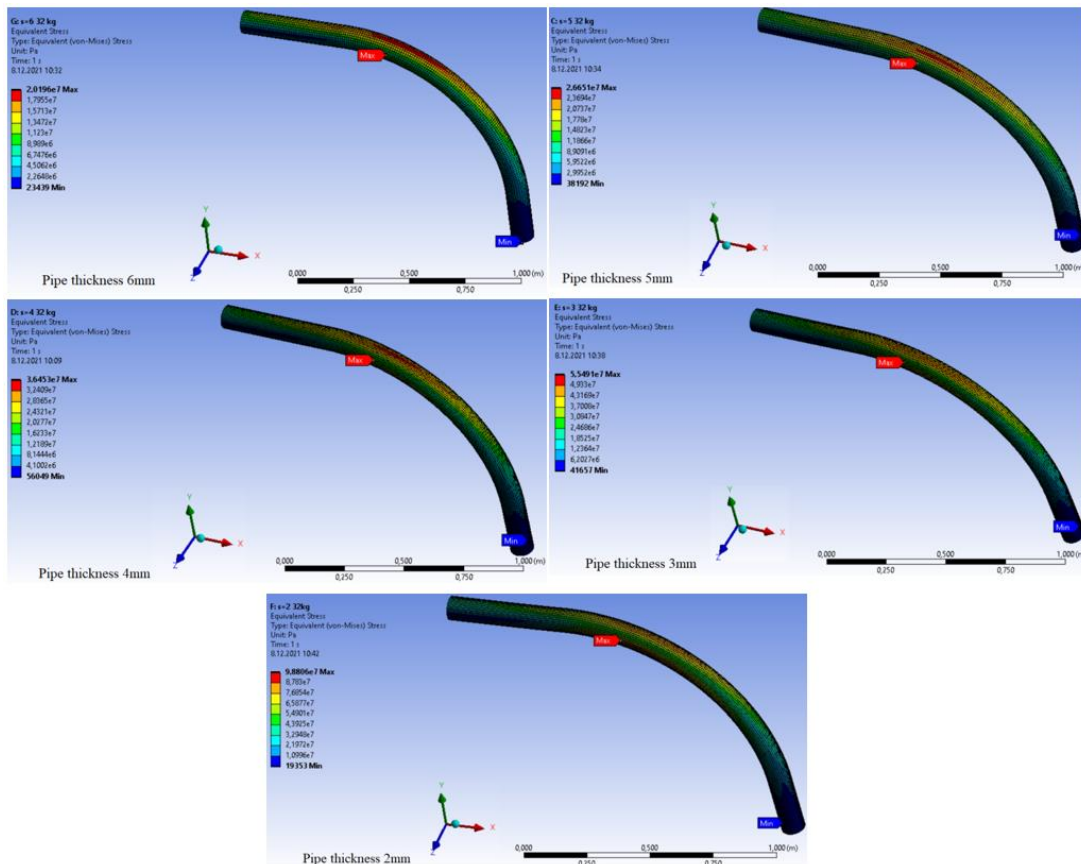


Figure 6. Total deformations in rotating arms with different pipe thickness

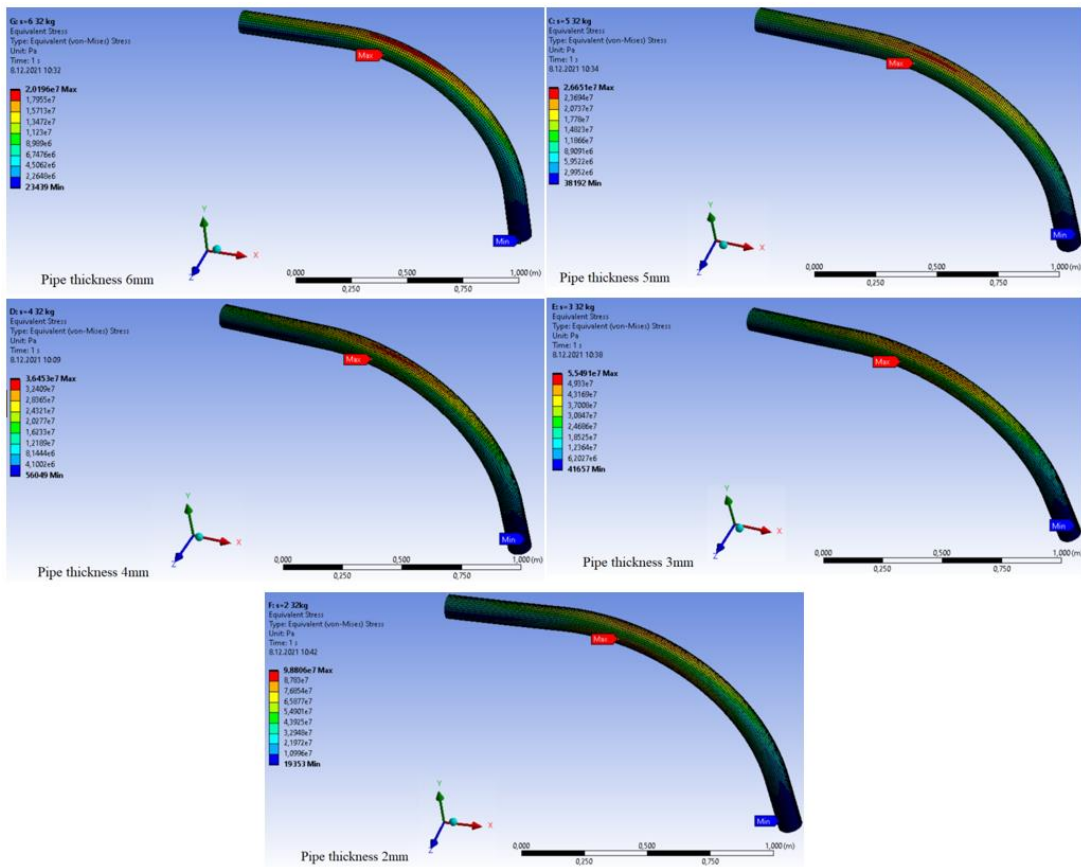


Figure 7. Stress changes in rotating arms with different pipe thicknesses

The mesh structure was obtained as shown in Figure 5. In the model with a mesh structure, the rotating arm was fixed in the flange side where hydromotor was mounted to rotate the arms. The force to be applied to the rotating wrapping arm was determined by considering the maximum operating pressure, torque of the hydromotor and the force that comes to the stretch wrap during the movement of the machine using the above-mentioned equations. 1009.7 N force was applied to the rotating arm in the form of a distributed load. A total of 52995 nodes and 7854 elements were created in the model for 5mm pipe thickness.

3. Results and Discussion

Depending on the weight of the bale and the stretch, the force on the rotating arm was applied as a distributed load. Depending on the force on the rotating arm, problems arise in the machine and different deformation problems can be seen. In order for the rotating arm to do its job in the best way, its strength should be increased. At this point, the thickness of the pipe has been changed for the optimization of the rotating arm driven by the hydromotor. For five different pipe thicknesses, points and amounts of maximum deformation, minimum and maximum stresses were examined. Figure 6 shows the total deformation of the rotating arms with different pipe thicknesses.

As seen in Figure 6, the minimum displacement is seen on the flange side where the hydromotor is connected. Maximum deformation was observed in the part where the stretch to which the load is applied is connected. It is seen that the maximum deformation

decreases as the pipe thickness of the rotating arm increases.

During the wrapping of the bale, the force applied to the stretch and the rotating arm may cause bending and deformation of the rotating arm. At this point, the bale cannot be effectively wrapped with a stretch. Figure 7 shows the points where the minimum and maximum stress occurs. In addition, the amounts of the minimum and maximum stresses in the rotating arm with different pipe thicknesses have been also given. It is seen that the minimum stress in the rotating arms is observed where the stretch is attached. It is seen that the maximum stress in all rotating arm designs is in the bending part of the pipe. In the analysis results, it is seen that the maximum stress decreases as the pipe thickness increases. Table 3 shows the minimum and maximum displacement and stress values obtained in the designed rotating arms.

Table 3. Minimum and maximum displacement and stress values obtained in the designed rotating arms

Pipe thickness (mm)	Maximum displacement (mm)	Minimum Stress (MPa)	Maximum Stress (MPa)	Maximum Shear Stress (MPa)
6	2.2677	0.0235	20.196	11.658
5	2.9035	0.0319	26.651	15.321
4	3.9552	0.0560	36.453	20.747
3	6.0299	0.0416	55.491	30.805
2	11.636	0.0194	98.806	52.846

4. Conclusions

In this study, the design optimization of the rotating arms of the bale wrapping machine has been carried out. Without changing the length and radius dimensions of the rotating arms, the rotating arms with pipe thicknesses of 6,5,4,3 and 2 mm were modeled. The force applied to the stretch and rotating arm during the wrapping of the bale was determined. The determined force was applied to the rotating arms. Structural static analyzes of the designed rotating arms of different sizes were carried out in the Ansys Workbench program. Analysis results showed that the amount of deformation decreases as the pipe thickness of the rotating arm of the winding machine increases. Maximum deformation is seen with the rotating arm with a pipe thickness of 2 mm. In addition, the analysis shows that the maximum stress decreases as the pipe thickness increases. As a result of the study, the stresses occurring in the rotating arm of the bale wrapping machine were determined and the optimum rotating arm design was tried to be determined. Safety factor has been determined as 8.817, 6.446, 4.234 and 2.378 for 5, 4, 3 and 2 mm pipe thickness. It can be suggested that 3mm pipe thickness could be safely used for rotating arms. It has been observed that as the pipe thickness increases, the stresses occurring in the rotating arm decrease and the pipe strength can be increased.

Acknowledgment

This study is supported by Kosgeb (Small and Medium Enterprises Development and Support Administration) in frame of the project name of Design and Development of Trailed Type Roll Baler carried out by Kayhan Ertuğrul Machinery Industry and Trade Inc. As researchers; we thank the KOSGEB and KAYHAN ERTUĞRUL MACHINERY INDUSTRY and TRADE INC.

Nomenclature

M_{ab}	:Torque of hydromotor (Nm)
ΔP	:Pressure difference (bar)
V	:Displacement (cm ³)
η_{mh}	:Hydromechanical efficiency
P_{ab}	: Engine power (kW)
Q	: Flow rate (L/min)
η_{ges}	: Total efficiency
n	: Hydromotor speed (rpm)
η_v	: Volumetric efficiency
F	: Force (N)
T	: Torque (Nm)

Conflict of Interest Statement

The authors declare that there is no conflict of interest in the study.

CRedit Author Statement

Soner Duran: Project administration, Data curation, Formal analysis, Methodology, Funding acquisition **Yasin Coşkun:** Conceptualization, Supervision, Funding acquisition, Investigation, Resources, **Derya Kılıç:** Conceptualization, Supervision, Funding acquisition, Roles/Writing –original draft, Resources **Ahmet Uyumaz:** Writing-review&editing, Conceptualization, Methodology, Investigation, Supervision, **Batuhan Zengin:** Data curation, Investigation, Visualization, Validation, Software

References

1. Bilgen H, Yalçın H, Özkul H, Çakmak B, Polat M, Kılıç A (2005). The effects of plastic color, vacuum implementation and holding method on the quality of packaged corn silage feed. *Ege Üniversitesi Ziraat Fakültesi Dergisi*, 42(2), 77-85.
2. Wood, Brian J. B. *Microbiology of fermented foods Volume 1&2*. Springer. s. 73.
3. Geren H., Avcioglu R., Kır B., Et Al. (2003). The Effect of Different Seed Times on Yield and Quality Features in Some Corn Varieties Cultivated as Second Crop Silage. *Ege Üniversitesi Ziraat Fakültesi Dergisi*, 40(3):57-64.
4. Ayık, M. (1993). *Hayvancılıkta Mekanizasyon*. (II. Baskı). Ankara Üniversitesi Ziraat Fakültesi Yayınları: 1300. Ders Kitabı 375, Ankara.
5. Muck, R. E., Nadeau, E. M. G., McAllister, Et Al. (2018). Silage review: Recent advances and future uses of silage additives. *Journal of dairy science*, 101(5), 3980-4000.
6. McDonald, P., Henderson, A. R., Heron, S. J. E. (1991). *The biochemistry of silage*. Chalcombe publications.
7. Martinson K, Coblenz W, Sheaffer C. (2011). The effect of harvest moisture and bale wrapping on forage quality, temperature, and mold in orchard grass hay. *Journal of Equine Veterinary Science*, 31(12): 711–716.
8. Coblenz W K, Coffey K P, Chow E A. (2016). Storage characteristics, nutritive value, and fermentation characteristics of alfalfa packaged in large-round bales and wrapped in stretch film after extended time delays. *Journal of Dairy Science*, 99(5): 3497–3511.
9. Taylor, R. K., Blasi D A, Shroyer J P. (1994). Storage losses in net-wrapped, large round bales of alfalfa. *Applied Engineering in Agriculture*, 10(3): 317–320.
10. Taşkaya, S. (2018). St 37 Çeliğinin Ansys Programında Basınca Bağlı Olarak Mekanik Gerilmelerin İncelenmesi. *The Journal of International Manufacturing and Production Technologies*. 39-46.
11. <https://www.esb-group.com/en/products-din-en/structural-grade-carbon-steel/>
12. <https://metalitec.zriha.com/eng/raw-materials/st37>